PERIODICO di MINERALOGIA
established in 1930

Dipartimento di Scienze della Terra
Sapienza Università di Roma

An International Journal of
Mineralogy, Crystallography, Geochemistry,
Ore Deposits, Petrology, Volcanology
and applied topics on Environment, Archaeometry and Cultural Heritage

Synchrotron radiation methods for studying biological interaction of fibres: an overview

Simona Raneri [1], Laura Fornasini [1,2], Danilo Bersani [2], Serena Mirata [3], Alessandra Gianoncelli [4,*]

[1] CNR-ICCOM, Consiglio Nazionale delle Ricerche, Istituto di Chimica e dei Composti OrganoMetallici, Via G. Moruzzi 1, 56124 Pisa, Italy
[2] Department of Mathematical, Physical and Computer Sciences, University of Parma, Parco Area delle Scienze 7/A, 43124 Parma, Italy
[3] Department of Experimental Medicine, University of Genova, Via Leon Battista Alberti 2, 16132 Genova, Italy
[4] Elettra - Sincrotrone Trieste, Strada Statale 14, km 163.5 in Area Science Park, 34149 Basovizza-Trieste, Italy

ARTICLE INFO

Submitted: May 2023
Accepted: June 2023
Available on line: July 2023

* Corresponding author:
alessandra.gianoncelli@elettra.eu

Doi: 10.13133/2239-1002/18090

How to cite this article:
Raneri S. et al. (2023)
Period. Mineral. 92, 179-190

ABSTRACT

In the last decade, synchrotron-based techniques have emerged as effective tools for investigating biological systems at the sub-cellular level. In asbestos-related studies, X-ray microscopy, combined with X-ray Fluorescence (XRF) and X-ray absorption near edge structure (XANES) enable successfully investigating the interaction between fibres and cells. Microscopy and chemical imaging provide very detailed maps, thus chemically and morphologically characterizing the biological interaction of fibres while monitoring different toxicity mechanisms. Additionally, the combination of microchemical and structural information can clarify metal mobilization processes, highlighting both their intracellular spatial distribution and the possible changes in their valence state induced by the fibres-cells interaction.

The activities within the PRIN 2017-FIBRES project included the utilization of multidisciplinary techniques and expertise to study the interaction of different fibres (chrysotile, erionite and crocidolite) with THP-1-derived macrophages. The numerous experiments carried out at TwinMic (Elettra synchrotron, Trieste, Italy) and ID21 (ESRF, Grenoble, France) beamlines - here discussed and generally presented - offered the opportunity to review the invaluable contribution of synchrotron-based techniques in studying mineral fibres and their biological interaction to step forward in the understanding of asbestos toxicity and carcinogenicity.

Keywords: SR-μXRF; SR-μXANES; TwinMic; ID21; asbestos; THP-1 cells.

INTRODUCTION

In the frame of the PRIN 2017 - FIBRES project, *in vitro* experiments were conducted using macrophages exposed to mineral fibres to evaluate the extent of their cellular toxicity (Mirata et al., 2022). Three carcinogenic mineral fibres were selected for the investigation, namely chrysotile (Balangero, Turin, Italy) (Pollastri et al., 2016a; Fornasini et al., 2022), crocidolite UICC standard sample (South Africa) (Pacella et al., 2019), and fibrous erionite (Jersey, Nevada, USA) (Gualtieri et al., 2016); human monocytic cell lines THP-1 were exposed to these fibres monitoring their interaction at different time intervals (i.e., 8 h, 24 h, 96 h).

When investigating the viability of biological systems exposed to fibres, a preliminary characterization of the fibres and other mineralogical phases is of paramount importance for the identification of mineral compounds that may be responsible for metal release associated with fibres dissolution.

Iron-bearing compounds are commonly present and may

occur as oxides, oxyhydroxides, carbonates or sulphides. As iron content needs to be considered in the toxicity of asbestos fibres, the detection and the identification of these impurities may be relevant to correlate the role of iron with its origin, whether from the fibres or from other impurities. Micro-Raman spectroscopy has been proven to be an effective tool for the characterization of mineral fibres and other mineralogical phases present in asbestos. Noteworthy, micro-Raman characterization of asbestos materials may be performed in biological systems (e.g., with THP-1 macrophages) (Mirata et al., 2022; Bassi et al., 2023) since mineral fibres can be identified by their distinctive Raman spectra (Petriglieri et al., 2015; Fornasini et al., 2022). Concerning iron-bearing compounds, different oxides and oxyhydroxides can be distinguished (such as magnetite, hematite, ilmenite, lepidocrocite); iron carbonates and iron sulphides may be found in different forms (Fornasini et al., 2022).

The study of the early responses of human non-differentiated and differentiated macrophages to the three carcinogenic mineral fibres through *in vitro* tests allowed the examination of the relationship between the toxicity parameters and the subsequent toxicity mechanism leading to severe lung diseases (Mirata et al., 2022). Among others, the release of metals in both intra- and extracellular environments represents an interesting mechanism to be fully investigated, also in relation to biodurability, fibres dissolution and toxic metal cargo release. However, a complete investigation of cell-fibres systems requires both the identification of metals released in the cellular environment and the study of their spatial distribution. In this perspective, synchrotron-based methods have emerged as an effective tool for investigating biological systems at the sub-cellular level (Pascolo et al., 2013; Pascolo et al., 2015; Cammisuli et al., 2018; Gianoncelli et al., 2019). The brilliant and tunable synchrotron source selected at different wavelengths and focused at specifically equipped endstations enables obtaining both qualitative and quantitative analysis of biosamples, reaching micro- or nanometric resolution and even combining different analytical techniques.

When studying the interaction between mineral fibres and the cellular environment, elemental and structural techniques are required to determine the chemical composition of biological and geological samples, or to discriminate the chemical speciation, respectively (Gherase and Fleming, 2020). When used in conjunction with mapping capabilities, micro- or nano-beam techniques can be used to spatially resolve such information.

Synchrotron radiation X-ray fluorescence micro-mapping (SR-μXRF) techniques enable the acquisition of chemical images describing the co-localization of specific chemical elements. X-ray probes focused at the sample generate X-ray fluorescence photons, characteristics of the excited chemical element; when coupled with high-resolution microscopy, high-resolution absorption and phase contrast images (i.e., morphological images) are simultaneously acquired and correlated with the chemical maps. For studying biological systems, both soft and hard X-ray microprobes appear suitable in function of the elements of interest, taking advantage of the range of spatial resolution and detection limits provided by different endstations available at the worldwide synchrotron facilities (Table 1).

The distribution of metals in intra- and extracellular environments can be easily mapped by SR-μXRF on different kinds of biosamples, from plants to cells and tissues (Bohic et al., 2008; Pascolo et al., 2011; Majumdar et al., 2012; Paunesku et al., 2012, Kopittke et al., 2014; Bonanni and Gianoncelli, 2023). For instance, SR-μXRF combined with soft X-ray Microscopy makes it possible to chemically and morphologically characterize the asbestos accumulated in the tissues (Pascolo et al., 2011, 2013, 2015, 2016a, 2016b) or in cells (Cammisuli et al., 2018; Gianoncelli et al., 2019) and to evaluate at the same time the biological response they cause. Indeed, XRF allows the study of the chemical interaction of pollutants with the elements and molecules of the lung by providing a real mapping of the chemical elements contained in a sample. High-resolution X-ray imaging, such as microtomography, has also been demonstrated to be an extremely useful approach for imaging asbestos bodies in lung tissues (Bardelli et al., 2021) but it does not provide chemical information.

Possible structural changes undergone by the fibres or associated mineral phases in relation to the contact time and biological environment can be studied by synchrotron X-ray absorption spectroscopy (SR-μXANES) technique (Ortega et al., 2012; Porcaro et al., 2018), by interpreting the photoabsorption behavior of a metal in its absorption edge region. Information on the oxidation state of chemical elements is particularly relevant when studying the release of metal cargos during fibres dissolution (Pascolo et al., 2013; Bardelli et al., 2023), thus clarifying the impact of cellular environment (e.g., pH values, etc.) in determining the changes of metal valence state (Ortega et al., 2009).

The refinement of crystal structures of carcinogenic fibres (Giacobbe et al., 2023), the determination of crystallinity of the fibres after interaction with cellular environments (Pollastri et al., 2016b; Gualtieri et al., 2017; Bardelli et al., 2023), the identification of associated mineral phases and the presence of impurities in crystal structures (Gualtieri et al., 2016) would need specific crystallo-chemical diffraction techniques (SR-μXRD)

Table 1. List of synchrotron beamlines suitable for simultaneous morphological and chemical studies on cells exposed to nanomaterials, with the indication of available techniques and some practical and useful set-up information.

Facility	Beamline	Energy range [keV]	Beam size [μm]	Techniques	Sample environment	Cryo stage
Advanced Light Source (ALS), USA	11.0.2	0.160-2	0.025	STXM, μXANES	Vacuum	No
APS, USA	26-ID	6-12	0.03 x 0.03	μXRF, μXRD	Air	No
Australian Synchrotron, Australia	Nanoprobe*	5-25	0.06 – 0.25	μXRF, μXANES, ptychography, XRF tomography	Air or vacuum (for cryo)	Yes
CLS, Canada	SM	0.13-2.7	0.03	μXRF, μXANES, STXM	Vacuum	Yes
CLS, Canada	SGM	0.25-2	1 x 0.1	μXRF, μXANES	Vacuum	Yes
DESY, Germany	P06	8-30	0.05 – 0.35	μXRF, μXANES, ptychography, XRF tomography	Air	No
Diamond, UK	I08	0.2-4.2	0.1 - 2	μXRF, μXANES, STXM	Vacuum	Yes
Elettra, Italy	TwinMic	0.4-2.2	0.1 - 2.5	μXRF, μXANES, STXM, ptychography	Vacuum	No
ESRF, France	ID16B	6-65	0.05 x 0.05	μXRF, μXANES, μXRD	Air	No
ESRF, France	ID21	2-11	0.03 x 0.07	μXRF, μXANES, μXRD	Vacuum	Yes
MAXIV, Sweden	NanoMAX	6-28	0.05 -0.2	μXRF, μXANES, ptychography	Air	No
MAXIV, Sweden	SoftiMAX	0.275-2.5	0.01 -0.1	μXRF, μXANES, STXM	Vacuum	No
NSLS II, USA	HXN	12-17	0.1 - 0.4	μXRF, μXANES, μXRD, 3D XRF	Air	No
Soleil, France	Hermes	0.07-2.5	0.025	STXM, μXANES	Vacuum	Yes
SOLEIL, France	Nanoscopium	5-20	0.05 - 1	μXRF, μXANES, μXRD	Air	No
Paul Scherrer Institute (PSI), Switzerland	Pollux	0.25-1.6	0.02	STXM, μXANES, ptychography	Vacuum	No
Pohang Light Source (PLS), Korea	10A	0.1-2	0.025	STXM, μXANES	Vacuum	No
Shanghai Synchrotron Radiation Facility (SSRF), China	BL08U1-A	0.25-2	0.3	STXM, μXANES	Vacuum	No

* newly open to users or under design/construction.

whose spectrum of applications, handling of samples and processing of diffraction data is continually improved at synchrotron radiation sources both for biological and geological studies (Gräfe et al., 2014).

In the present work, the potentiality of combining elemental and structural information through the application of SR-μXRF and SR-μXANES on fibre-cell systems is discussed, following successful approaches

reported in the literature (Pascolo et al., 2013; Bardelli et al., 2023).

BIOSAMPLE PREPARATION

According to the desired application, specific sample preparation is required for the different synchrotron-based techniques (i.e., SR-μXRF, SR-μXANES, SR-μXRD). Indeed, the preservation of the elemental distribution is fundamental for imaging techniques such as SR-XFM (Synchrotron Radiation X-ray Fluorescence Mapping), whereas the preservation of the chemical form is critical for techniques focusing on elemental speciation such as XANES and X-ray Absorption Spectroscopy (XAS) (Sarret et al., 2013).

In cryogenic fixation protocols like plunge-freezing and high-pressure freezing, sample fixation is characteristically achieved within milliseconds, resulting in the simultaneous immobilization of all macromolecular components thus preserving their native state. In the plunge-freezing method, the sample is plunged in a cryogen (i.e., propane, ethane, or isopentane) cooled with liquid nitrogen (Vogel-Mikuš et al., 2009). This protocol is particularly effective for elemental mapping and speciation, although it is better suited for small samples (<0.6 mm diameter) since the cooling rates decrease as sample size increases (Isaure et al., 2015). In high-pressure freezing, the fast cooling of the sample (~20 ms) happens at high pressure (~2100 bars), inhibiting the expansion of water and thus the formation of ice crystals. The resulting fast and homogenous freezing allows optimal ultrastructure preservation, while the automation of this process ensures its high reproducibility. Nonetheless, this method requires the use of expensive instrumentation and it is restricted to small samples of a few mm (McDonald, 2009; Lambrecht et al., 2015).

In case the beamline does not have a cryogenic stage or a fast detector, it is of paramount importance to dehydrate the cryofixed samples to avoid ice melting and recrystallization. This process is usually carried out by freeze-drying the samples at the lowest temperature possible under low pressure (~10^{-2} mbar) before they are gradually brought back to room temperature and pressure. However, if this process is not properly done, it may result in elemental redistribution, loss of elements, shrinking of the specimens and severe morphology distortion. To avoid sample shrinkage and/or distortion, critical point drying may be preferred to remove water from the sample. In fact, in critical point drying the transitional medium is CO_2 (critical point at 31 °C, 73.8 bar), although an intermediate step in which water is replaced by acetone, methanol, ethanol, or amyl acetate is necessary since CO_2 and water are not miscible (Castillo-Michel et al., 2017).

As an alternative to cryofixation protocols, chemical fixation is a widely employed technique based on chemical fixatives, such as formalin, formaldehyde, paraformaldehyde, or glutaraldehyde (Castillo-Michel et al., 2017). However, it has been evidenced that, although it usually preserves the ultrastructure of the sample, chemical fixation may lead to elemental redistribution and loss of content. In particular, it has been reported that sample fixation with formalin prompted the redistribution of K, Ca, Fe, Cu and Zn (Chwiej et al., 2005; Hackett et al., 2011; Punshon et al., 2015; Zohdi et al., 2015), whereas sample preparation with paraformaldehyde or methanol induced poor preservation of intracellular Mg and K (Perrin et al., 2015; Merolle et al., 2023).

CHEMICAL SPECTROSCOPIES USING SYNCHROTRON RADIATION

Among other research focuses, metals mobilization and fibres dissolution mechanisms are in the light of the PRIN 2017-FIBRES project's scopes. In this field, the investigations aim at identifying the composition of the dissolution products and their origin, possibly determining when related to fibres dissolution or to the interaction of associated mineral compounds - especially iron-bearing species - with biological material. With these premises, Synchrotron Radiation X-ray Fluorescence Mapping and μXANES were coupled to map and analyze metal speciation in different macrophages-fibres systems from the beginning of the interaction (8 h) over medium exposure times (24 h and 96 h).

The range of metals involved in dissolution mechanisms (e.g., from Mg to Cr in the case of chrysotile fibre dissolution and metal cargo release) required the combined use of soft and hard X-ray sources, accessible at specific endstations. The TwinMic soft X-ray microscope (Gianoncelli et al., 2016) at Elettra Sincrotrone Trieste (Trieste, Italy) combines scanning transmission X-ray Microscopy (STXM) with low energy XRF in the 400-2200 eV energy range allowing elemental mapping of light elements, from B to P, and transition metals, such as Mn, Fe, Ni, Co, Cu and Zn (Gianoncelli et al., 2013), while the recently updated ID21 beamline at ESRF synchrotron (Grenoble, France) provides complementary elemental mapping combined with μXANES spectroscopy by working in the 2-9.5 keV energy range (Salomé et al., 2013; Cotte et al., 2017). Both beamlines can operate at submicron spatial resolution, well suited for cell-fibre systems' studies. All XRF spectra were processed with the PYMCA software package (Solé et al., 2007).

In this examination of THP-1-derived macrophages exposed to three carcinogenic mineral fibres, namely chrysotile (Balangero, Italy), crocidolite UICC (South Africa) and Na-erionite (Jersey, USA), we illustrate the kind of information that can be obtained by using two different beamlines and taking advantage of the

complementarity of μXANES-μXRF spectroscopies, by presenting some examples.

For our experiments with human THP-1-derived macrophages, 200 nm thick silicon nitride (Si_3N_4) membranes with a frame of 5 mm x 5 mm and a membrane size of 1.5 mm x 1.5 mm were prepared for tissue culture according to Bissardon et al. (2019). Briefly, the silicon nitride membranes were sterilized with UVC light for 30 min and coated by adding 30 μL of poly-D-lysine on the flat surface of the membranes, which were then incubated for 25 min in a standard tissue culture incubator at 37 °C in a humidified 5% CO_2 atmosphere. After the membranes were washed three times with sterile deionized water to remove excess poly-D-lysine, they were left to dry overnight under a laminar flow hood. Then, THP-1 monocytes were seeded at 50,000 cells/membrane in a complete RPMI-1640 medium supplemented with 20 ng/mL of phorbol-12-myristate 13-acetate (PMA, PeproTech EC, London, UK). Thus, the membranes were placed in a 48-well plate with their flat side facing up and a 30 μL drop containing 50,000 cells was seeded on each membrane. After 30 min at 37 °C, the rest of the medium was added to the wells and THP-1 monocytes were induced to polarise into either M0 or M1 macrophages as described in Mirata et al. (2022). THP-1-derived macrophages were then treated with 50 μg/mL of crocidolite UICC (South Africa), chrysotile (Balangero, Turin, Italy) and Na-erionite (Jersey, Nevada, USA) for 8 h, 24 h, or 96 h. Then, the cells were washed twice with PBS and fixed with 4% paraformaldehyde in PBS for 30 min at room temperature. After the paraformaldehyde was completely removed by gently washing the membranes with sterile deionised water, the silicon nitride membranes were dried under a laminar flow hood.

SR-μXRF mapping. Metal release from fibres and associated minerals: the example of iron

The content of iron in mineral fibres has a fundamental role in the formation of reactive oxygen species (ROS) since it is directly involved in the generation of hydrogen peroxide (H_2O_2) and hydroxyl radicals (HO•) via the Haber-Weiss cycle and the Fenton reaction (Gualtieri et al., 2019a; Gualtieri, 2021).

In chrysotile, several iron-bearing species are commonly found as impurities. Iron is also substituent for magnesium in the octahedral sites of chrysotile or other serpentine polymorphs (e.g., antigorite), which are generally found as accessory phases in chrysotile fibres (Pollastri et al., 2016a). Furthermore, iron is a constitutive element in balangeroite, a fibrous inosilicate present within chrysotile fibres from Balangero (Italy) (Fornasini et al., 2022). Non-fibrous species containing iron were also typically observed in chrysotile. For example, in chrysotile from Balangero (Italy), they consist mainly of iron oxides and oxyhydroxides (e.g., magnetite, hematite, ilmenite, lepidocrocite), iron sulphides (e.g., mackinawite and iron-nickel sulphides) or iron carbonates (containing also magnesium) (Fornasini et al., 2022). In crocidolite, the presence of surface iron (either Fe^{2+} or Fe^{3+}) has to be considered. As observed in crocidolite UICC, iron-bearing impurities can be found as minor amounts of hematite, magnetite, siderite, minnesotaite (Pacella et al., 2019).

In vitro THP-1-cellular studies with chrysotile fibres, reporting the contribution of iron in cellular mortality, demonstrated the formation of aggregated structures of both fibrous and non-fibrous species. Clusters (from a few tens μm up to >100 μm wide) of organic and inorganic materials were observed near the THP-1 cells, including both fibrous and non-fibrous species; as clusters size and concentration rise in prolonged exposure times (exceeding 100 μm size after 96 h exposure), these products were still observed, though hardly distinguishable, suggesting a partial dissolution of the inorganic material.

Understanding the spatial distribution of iron both on the surface of mineral fibres and in other mineralogical impurities is therefore essential to evaluate the metal release dissolution in biological systems (Gualtieri et al., 2019a).

In Figures 1 and 2 absorption images and SR-μXFM maps collected on different THP-1 phenotypes at the beginning and the end of monitoring time outlined the progressive interaction of the chrysotile fibres and associated minerals with cells.

Overall, the morphology of mineral fibres and associated accessory phases can clearly be distinguished. Chrysotile fibres, iron sulphides (i.e., mackinawite) and iron oxides (i.e., magnetite) particles are detected in Figure 1, as recognized with preliminary micro-Raman measurements by their characteristic spectra; in Figure 1b, a balangeroite fibre is highlighted. The different morphology of chrysotile and balangeroite fibres is clear from the absorption images, proving the curvilinear shape of chrysotile fibres against the rigid profile of balangeroite.

Looking at the selected elements, Na and P outline cells due to their high content in the intracellular environment and in the DNA, respectively; Fe marks fibres and accessory mineral particles, and the extent of metal release into the biological system.

In M0-THP-1 cells treated with chrysotile (Figure 1), the mapped areas correspond to clusters of fibres and particles with cellular material. At increasing exposure times, the release of Fe is clearly highlighted. After 8 h exposure time, Fe is mainly localized on fibres and particles, whereas after 24 h higher Fe content is observed both on fibres and diffusely around them; at increased

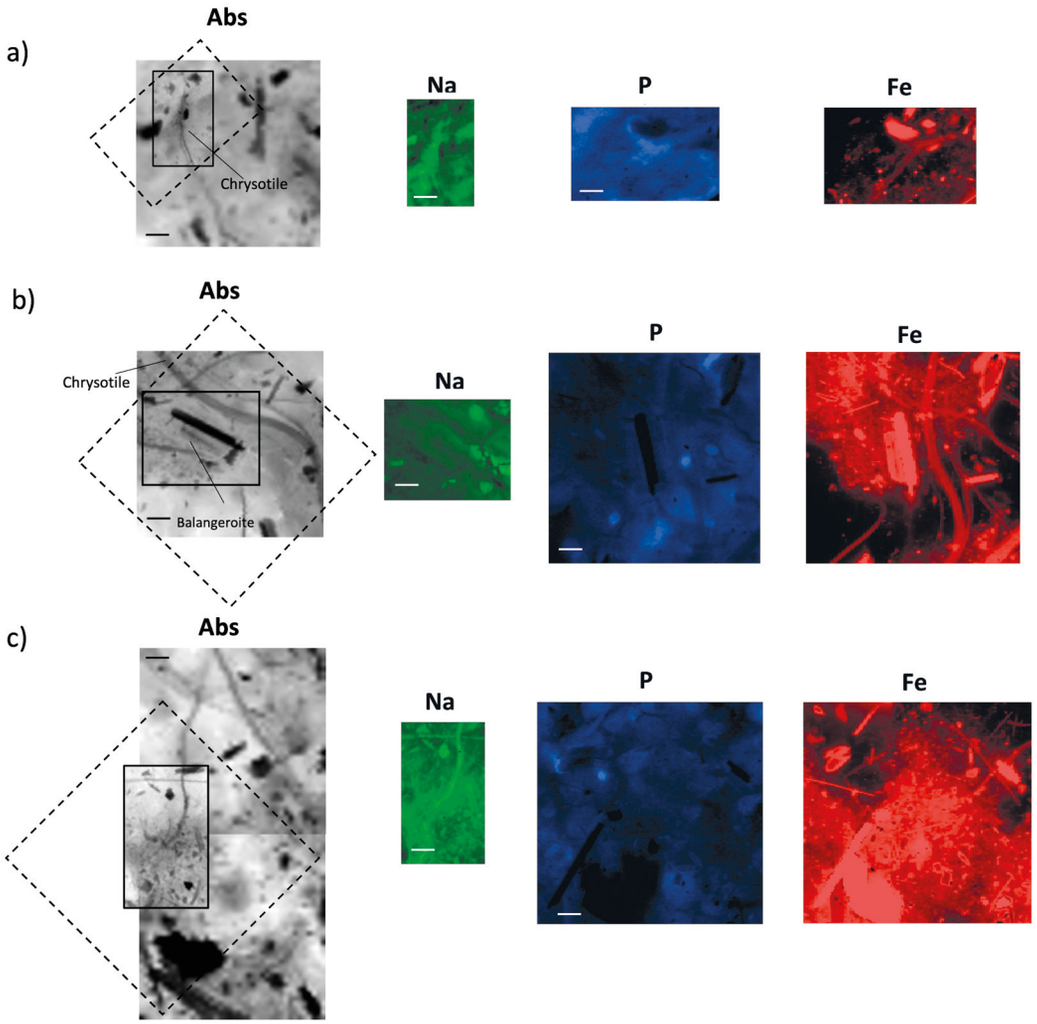

Figure 1. Absorption (Abs) images and corresponding elemental maps collected on M0-THP-1 macrophages treated with chrysotile after (a) 8 h, (b) 24 h and (c) 96 h of contact with fibres. Maps of Na were collected at TwinMic beamline (Elettra) (ROIs marked by continuous line) at 1500 eV excitation energy, while P and Fe were collected at ID21 beamline (ESRF) (ROIs marked by dot line) at 7.3 keV excitation energy. Scale bars are 10 µm.

exposure time (96 h), Fe is extensively widespread in the cluster and the shape of the fibres is hardly distinguished.

In Figure 2a, the investigated area reports in the left part of the absorption image a cluster of fibres and particles after 8 h exposure in M1-THP-1 macrophages, whereas cells can be recognized on the right and lower side. SR-µXFM maps depict the high concentration of Fe especially on non-fibrous particles (i.e., mackinawite and magnetite) and balangeroite fibres; into the clusters, Fe is quite widespread along with cellular material, as indicated by the co-localization of Fe with Na and P. At this stage, cell morphologies can still be clearly outlined by P maps. After 96 h of contact with fibres, the extent of the cluster is quite reduced and isolated groups of M1-THP-1 cells are hardly distinguished as a result of the progressive phagocytosis of mineral fibres and accessory mineral particles. Fe is mainly localized on balangeroite and iron-rich particles (sulfides and oxides), while chrysotile fibres - still recognizable into clusters and cells - are quite reduced in size; Fe is widespread and diffuses around them.

Considering the positive standard crocidolite (Cardile et al., 2004; Gualtieri et al., 2019b; Bernstein et al., 2020) herewith used for comparison, in THP-1 cells treated with crocidolite UICC standard (Figure 3), Fe and P maps enable the localization of fibres and cells, respectively, without evident metal release into the cellular environment at the beginning of the contact; after 96 h of exposure, Fe marks the numerous small fibres into the cells, evidencing the progress of phagocytosis

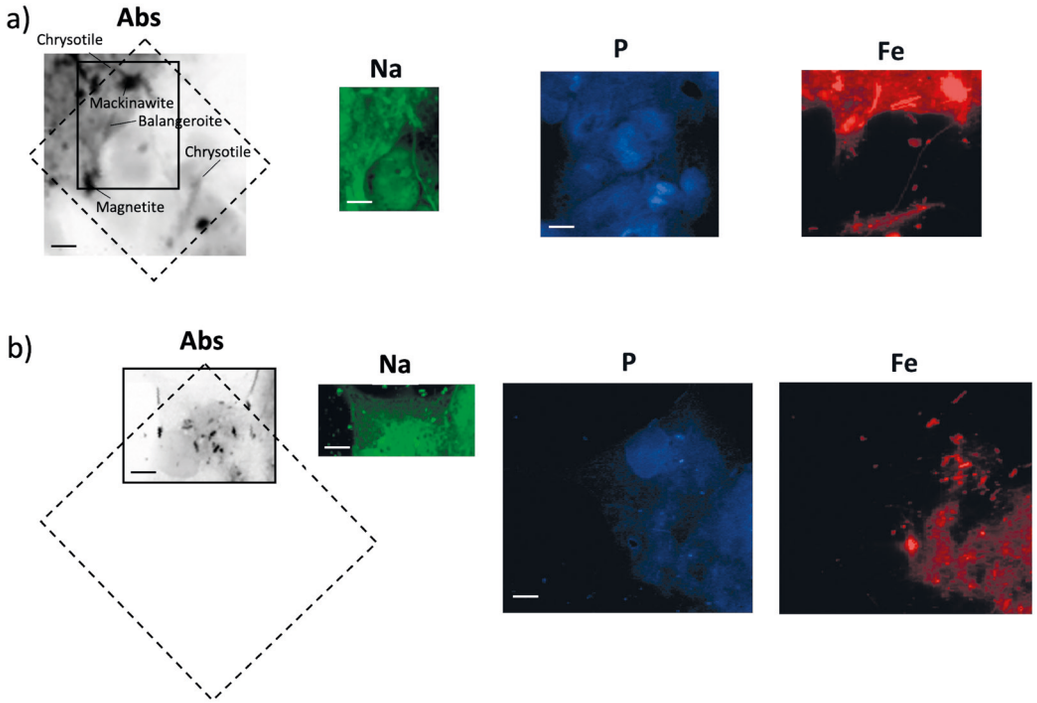

Figure 2. Absorption (Abs) images and corresponding elemental maps collected on M1-THP-1 macrophages treated with chrysotile after (a) 8 h and (b) 96 h of contact with fibres. Maps of Na were collected at TwinMic beamline (Elettra) (ROIs marked by continuous line) at 1500 eV excitation energy, while P and Fe were collected at ID21 beamline (ESRF) (ROIs marked by dot line) at 7.3 keV excitation energy. Scale bars are 10 µm.

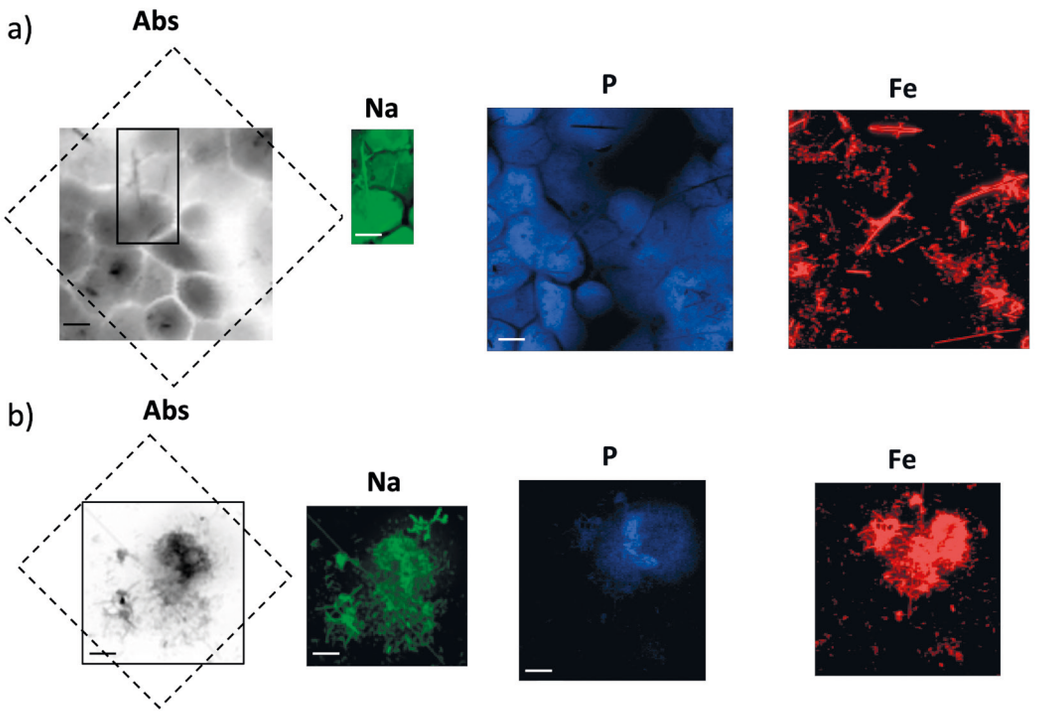

Figure 3. Absorption (Abs) images and corresponding elemental maps collected on M0-THP-1 macrophages treated with crocidolite after (a) 8 h and (b) 96 h of contact with fibres. Maps of Na were collected at TwinMic beamline (Elettra Sincrotrone Trieste) (ROIs marked by continuous line) at 1500 eV excitation energy, while P and Fe were collected at ID21 beamline (ESRF) (ROIs marked by dot line) at 7.3 keV excitation energy. Scale bars are 10 µm.

(Di Giuseppe et al., 2022). Contrary to chrysotile, Fe is not released into the biological environment, mainly as a result of the different biodurability of these two fibres.

These observations may seem counterintuitive when comparing the pristine content of Fe in crocidolite UICC standard (17.4 wt% FeO and 17.9 wt% Fe_2O_3) (Pacella et al., 2019) and in Balangero chrysotile (2.5 wt% FeO and 0.4 wt% Fe_2O_3) (Pollastri et al., 2016a). However, according to recent acellular dissolution tests, crocidolite and chrysotile exhibit very different biodurability rates in the macrophage phagolysosome environment; in fact, the estimated time of dissolution for chrysotile is extremely short in comparison to crocidolite (Gualtieri et al., 2018; Gualtieri et al., 2019c). As a result, although chrysotile contains a lower amount of iron in its structure, its low biodurability prompts the fast release of this metal in the extracellular and intracellular environments, as evidenced by the widespread diffusion of iron. Conversely, biodurable crocidolite releases its metals slowly, resulting in the detection of a lower amount of dispersed iron, despite its abundance within the fibres.

SR-μXANES. Iron speciation in fibrous-related impurities: the Na-erionite case

In order to investigate possible iron speciation changes in iron-rich impurities into the cellular environment, SR-μXANES spectroscopy was employed on selected points rich in iron in M1-THP-1 macrophages treated with Na-erionite (Jersey, Nevada, USA), previously identified by SR-μXRF mapping. Spectra were acquired at the ID21 beamline in XRF mode across the Fe K absorption edge and compared with suitable reference standards.

In particular, for all exposure times, XANES spectra were acquired on three typologies of iron-rich areas: i) particles located on fibres; ii) particles in proximity to fibres; iii) particles located into the cells. No significant differences were noticed among the three types of iron-rich regions in all exposure conditions (Figure 4) and no differences appeared when comparing 8 h with 24 h and 96 h of exposure. In all spectra, the main contributions resulted to be hematite and goethite, in agreement with Gualtieri et al. (2016), with a content of around 50% each, whereas no presence or negligible percentage of FeO is determined by the fitting process. Summarizing, no detectable speciation changes were evident from the spectra collected on the different areas in all conditions suggesting that iron particles associated with erionite fibres do not undergo chemical changes in this environment for the monitored exposure times.

CONCLUSIVE REMARKS

The systematic analysis of the biological interaction of three different carcinogenic fibres with different THP-1 phenotypes offered the opportunity to extend a combined SR-μXRF and SR-μXANES approach for investigating the mechanism of fibres dissolution and metal release of mineral fibres.

SR-μXRF and SR-μXANES data were demonstrated to be fundamental in defining the role of iron during fibre dissolution, highlighting the importance of accessory

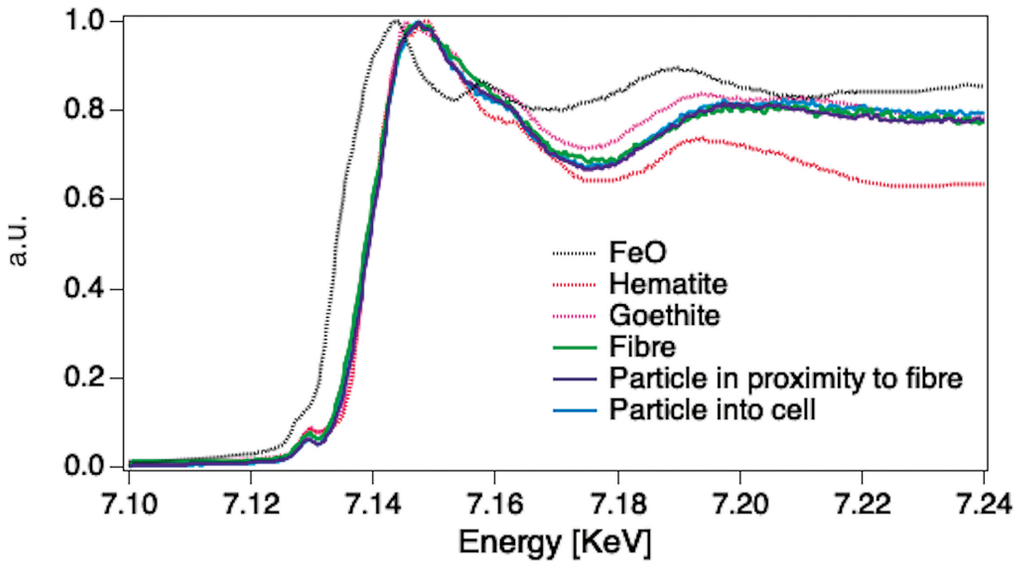

Figure 4. SR-μXANES spectra collected on particles and fibres in M1-THP-1 macrophages treated with Na-erionite, plotted together with goethite, hematite and FeO reference standards.

iron-rich minerals associated with different fibres.

In addition, synchrotron radiation - based experiments provide further insight in the results of *in vitro* tests; although all the three types of fibres are capable of causing lung diseases, they act through different toxicity mechanisms due to differences in the extent and type of metal release, in the release of toxic metal cargos, in the production of ROS and in the production of inflammatory mediators.

Overall, this systematic investigation represents an important step forward in the understanding of asbestos toxicity and pathogenicity, in particular clarifying the role of iron and other toxic metals in the surface activity of the fibres; the examples herewith reported depict only a representative collection of a wider investigation involving both metal release from fibres dissolution and metal cargo release, which will be the focus of dedicated forthcoming papers.

In conclusion, synchrotron-based methods have confirmed their relevant role in elucidating complex mechanisms at the sub-cellular level. They should be considered complementary to, rather than in competition with, standard laboratory approaches, since biological systems need to be studied from the mesoscale to the nanoscale in order to gain a more complete overview and understanding. With the advent of fourth-generation synchrotron sources, planned for almost all facilities, and relative beamlines' upgrades, we expect to see faster experiments combining multi-techniques in a more efficient way.

ACKNOWLEDGEMENTS

This work is supported by the PRIN 2017 funded project "Fibres: a multidisciplinary mineralogical, crystal-chemical and biological project to amend the paradigm of toxicity and cancerogenicity of mineral fibres" (PRIN: Progetti di Ricerca di Rilevante Interesse Nazionale-Bando 2017-Prot. 20173X8WA4). We are grateful to ESRF and Elettra synchrotrons for providing access to their facilities and to the beamlines (ID21: Exp. No LS-3076, doi:10.15151/ESRF-ES-744175308; Elettra: Exp. No 20215552, Exp. No 20225486). We are grateful to D. Di Giuseppe, V. Scognamiglio, S. Scarfi, V. Bonanni, E.E. Villalobos Portillo who participated in some experiment sessions.

REFERENCES

Bardelli F., Brun F., Capella S., Bellis D., Cippitelli C., Cedola A., Belluso E., 2021. Asbestos bodies count and morphometry in bulk lung tissue samples by non-invasive X-ray micro-tomography. Scientific reports 11, 10608.

Bardelli F., Giacobbe C., Ballirano P., Borelli V., Di Benedetto F., Montegrossi G., Bellis D., Pacella A., 2023. Closing the knowledge gap on the composition of the asbestos bodies. Environmental Geochemistry and Health, 1-13.

Bassi A.M., Mirata S., Almonti V., Tirendi S., Vernazza S., Fornasini L., Raneri S., Bersani S., Passalacqua M., Gualtieri A.F., Scarfì S., 2023. Cytotoxic and pro-inflammatory early effects of mineral fibres on human alveolar epithelial and immune cells. Periodico di Mineralogia, forthcoming.

Belluso E. and Ferraris G., 1991. New data on balangeroite and carlosturanite from Alpine serpentinites. European Journal of Mineralogy 3(3), 559-566.

Bernstein D.M., Toth B., Rogers R.A., Kling D.E., Kunzendorf P., Phillips J.I., Ernst H., 2020. Evaluation of the dose-response and fate in the lung and pleura of chrysotile-containing brake dust compared to TiO2, chrysotile, crocidolite or amosite asbestos in a 90-day quantitative inhalation toxicology study - Interim results Part 2: Histopathological examination, Confocal microscopy and collagen quantification of the lung and pleural cavity. Toxicology and Applied Pharmacology 387, 114847.

Bissardon C., Reymond S., Salomé M., André L., Bayat S., Cloetens P., Bohic S., 2019. Cell culture on silicon nitride membranes and cryopreparation for Synchrotron X-ray Fluorescence nano-analysis. Journal of Visualized Experiments: JoVE 154, e60461.

Bohic S., Murphy K., Paulus W., Cloetens P., Salomé M., Susini J., Double K., 2008. Intracellular chemical imaging of the developmental phases of human neuromelanin using synchrotron X-ray microspectroscopy. Analytical Chemistry 80, 9557-9566.

Bonanni V. and Gianoncelli A., 2023. Soft X-ray Fluorescence and Near-Edge Absorption Microscopy for investigating metabolic features in biological systems: A review. International Journal of Molecular Sciences 24, 3220.

Cammisuli F., Giordani S., Gianoncelli A., Rizzardi C., Radillo L., Zweyer M., Da Ros T., Salomé M., Melato M., Pascolo L., 2018. Iron-related toxicity of single-walled carbon nanotubes and crocidolite fibres in human mesothelial cells investigated by Synchrotron XRF microscopy. Scientific reports 8, 706.

Cardile V., Renis M., Scifo C., Lombardo L., Gulino R., Mancari B., Panico A., 2004. Behaviour of the new asbestos amphibole fluoro-edenite in different lung cell systems. The International Journal of Biochemistry & Cell Biology 36, 849-860.

Castillo-Michel H.A., Larue C., Pradas Del Real A.E., Cotte M., Sarret G., 2017. Practical review on the use of synchrotron based micro- and nano- X-ray fluorescence mapping and X-ray absorption spectroscopy to investigate the interactions between plants and engineered nanomaterials. Plant Physiology and Biochemistry 110, 13-32.

Chwiej J., Fik-Mazgaj K., Szczerbowska-Boruchowska M., Lankosz M., Ostachowicz J., Adamek D., Simionovici A., Bohic S., 2005. Classification of nerve cells from substantia nigra of patients with Parkinson's disease and amyotrophic lateral sclerosis with the use of X-ray fluorescence microscopy and multivariate methods. Analytical Chemistry 77, 2895-2900.

Cotte M., Pouyet E., Salome M., Rivard C., De Nolf W., Castillo-Michel H., Fabris T., Monico L., Janssens K., Wang T., Sciau P., Verger L., Cormier L., Dargaud O., Brun E., Bugnazet D., Fayard B., Hesse B., del Real A.P., Veronesi G., Langlois J., Balcar N., Vandenberghe Y., Sole V.A., Kieffer J., Barrett R., Cohen C., Cornu C., Baker R., Gagliardini E., Papillon E., Susini J., 2017. The ID21 X-ray and infrared microscopy beamline at the ESRF: status and recent applications to artistic materials. Journal of Analytical Atomic Spectrometry 32, 477-493.

Di Giuseppe D., Scarfì S., Alessandrini A., Bassi A. M., Mirata S., Almonti V., Ragazzini G., Mescola A., Filaferro M., Avallone R., Vitale G., Scognamiglio V., Gualtieri A.F., 2022. Acute cytotoxicity of mineral fibres observed by time-lapse video microscopy. Toxicology 466, 153081.

Fornasini L., Raneri S., Bersani D., Mantovani L., Scognamiglio V., Di Giuseppe D., Gualtieri A.F., 2022. Identification of iron compounds in chrysotile from the Balangero mine (Turin, Italy) by micro-Raman spectroscopy. Journal of Raman Spectroscopy 53, 1931-1941.

Gherase M.R. and Fleming D.E.B., 2020. Probing trace elements in human tissues with Synchrotron radiation. Crystals 10, 12.

Giacobbe C., Moliterni A., Di Giuseppe D., Malferrari D., Wright J.P., Mattioli M., Raneri S., Giannini C., Fornasini L., Mugnaioli E., Ballirano P., Gualtieri A.F., 2023. The crystal structure of the killer fibre erionite from Tuzkoy (Cappadocia, Turkey), International Union of Crystallography Journal, IUCrJ, 10(4), 1-14.

Gianoncelli A., Cammisuli F., Altissimo M., Salomé M., Radillo O., Ricci G., Giordani S., Rizzardi C., Pascolo L., 2019. Iron-related toxicity effects of single-walled carbon nanotubes in human placental cells (BeWo) investigated by X-ray fluorescence microscopy. X-Ray Spectrometry 48, 413-421.

Gianoncelli A., Kourousias G., Merolle L., Altissimo M., Bianco A., 2016. Current status of the TwinMic beamline at Elettra: a soft X-ray transmission and emission microscopy station. Journal of Synchrotron Radiation 23, 1526-1537.

Gianoncelli A., Kourousias G., Stolfa A., Kaulich B., 2013. Recent developments at the TwinMic beamline at ELETTRA: an 8 SDD detector setup for low energy X-ray Fluorescence. Journal of Physics: Conference Series 425, 182001.

Gräfe M., Klauber C., Gan B., Tappero R.V., 2014. Synchrotron X-ray microdiffraction (μXRD) in minerals and environmental research. Powder Diffraction 29(S1), S64-S72.

Gualtieri A.F., 2021. Bridging the gap between toxicity and carcinogenicity of mineral fibres by connecting the fibre crystal-chemical and physical parameters to the key characteristics of cancer. Current Research in Toxicology 2, 42-52.

Gualtieri A.F., Andreozzi G.B., Tomatis M., Turci F., 2019a. Iron from a geochemical viewpoint. Understanding toxicity/pathogenicity mechanisms in iron-bearing minerals with a special attention to mineral fibers. Free Radical Biology and Medicine 133, 21-37.

Gualtieri A.F., Bursi Gandolfi N., Pollastri S., Burghammer M., Tibaldi E., Belpoggi F., Pollok K., Langenhorst F., Vigliaturo R., Dražić G., 2017. New insights into the toxicity of mineral fibres: A combined in situ synchrotron μ-XRD and HR-TEM study of chrysotile, crocidolite, and erionite fibres found in the tissues of Sprague-Dawley rats. Toxicology Letters 274, 20-30.

Gualtieri A.F., Gandolfi N.B., Pollastri S., Pollok K., Langenhorst F., 2016. Where is iron in erionite? A multidisciplinary study on fibrous erionite-Na from Jersey (Nevada, USA). Scientific reports, 6, 37981.

Gualtieri A.F., Lusvardi G., Pedone A., Di Giuseppe D., Zoboli A., Mucci A., Zambon A., Filaferro M., Vitale G., Benassi M., Avallone R., Pasquali L., Lassinantti Gualtieri M., 2019b. Structure model and toxicity of the product of biodissolution of chrysotile asbestos in the lungs. Chemical Research in Toxicology 32, 2063-2077.

Gualtieri A.F., Lusvardi G., Zoboli A., Di Giuseppe D., Lassinantti Gualtieri M., 2019c. Biodurability and release of metals during the dissolution of chrysotile, crocidolite and fibrous erionite. Environmental Research 171, 550-557.

Gualtieri A.F., Pollastri S., Bursi Gandolfi N., Gualtieri M. L., 2018. In vitro acellular dissolution of mineral fibres: A comparative study. Scientific reports, 8, 7071.

Hackett M.J., McQuillan J.A., El-Assaad F., Aitken J.B., Levina A., Cohen D.D., Siegele R., Carter E.A., Grau G.E., Hunt N.H., Lay P.A., 2011. Chemical alterations to murine brain tissue induced by formalin fixation: implications for biospectroscopic imaging and mapping studies of disease pathogenesis. Analyst 136, 2941-2952.

Isaure M.-P., Huguet S., Meyer C.-L., Castillo-Michel H., Testemale D., Vantelon D., Saumitou-Laprade P., Verbruggen N., Sarret G., 2015. Evidence of various mechanisms of Cd sequestration in the hyperaccumulator Arabidopsis halleri, the non-accumulator Arabidopsis lyrata, and their progenies by combined synchrotron-based techniques. Journal of Experimental Botany 66, 3201-3214.

Kopittke P.M., Menzies N.W., Wang P., McKenna B.A., Wehr J.B., Lombi E., Kinraide T.B., Blamey F.P.C., 2014. The rhizotoxicity of metal cations is related to their strength of binding to hard ligands. Environmental Toxicology and Chemistry 33, 268-277.

Lambrecht E., Baré J., Claeys M., Chavatte N., Bert W., Sabbe K., Houf K., 2015. Transmission electron microscopy sample preparation protocols for the ultrastructural study of cysts of free-living protozoa. BioTechniques 58, 181-188.

Majumdar S., Peralta-Videa J.R., Castillo-Michel H., Hong J., Rico C.M., Gardea-Torresdey J.L., 2012. Applications of synchrotron μ-XRF to study the distribution of biologically important elements in different environmental matrices: a review. Analytica Chimica Acta 755, 1-16.

McDonald K.L., 2009. A review of high-pressure freezing

preparation techniques for correlative light and electron microscopy of the same cells and tissues. Journal of Microscopy 235, 273-281.

Merolle L., Pascolo L., Zupin L., Parisse P., Bonanni V., Gariani G., Kenig S., Bedolla D.E., Crovella S., Ricci G., Iotti S., Malucelli E., Kourousias G., Gianoncelli A., 2023. Impact of sample preparation methods on single-cell X-ray microscopy and light elemental analysis evaluated by combined low energy X-ray Fluorescence, STXM and AFM. Molecules 28(4), 1992.

Mirata S., Almonti V., Di Giuseppe D., Fornasini L., Raneri S., Vernazza S., Bersani D., Gualtieri A.F., Bassi A.M., Scarfì S., 2022. The acute toxicity of mineral fibres: A systematic in vitro study using different THP-1 macrophage phenotypes. International Journal of Molecular Sciences 23(5), 2840.

Ortega R., Carmona A., Llorens I., Solari P.L., 2012. X-ray absorption spectroscopy of biological samples. A tutorial. Journal of Analytical Atomic Spectrometry 27, 2054-2065.

Ortega R., Devès G., Carmona A., 2009. Bio-metals imaging and speciation in cells using proton and synchrotron radiation X-ray microspectroscopy. Journal of the Royal Society, Interface 6(Suppl 5), S649-S658.

Pacella A., Andreozzi G.B., Nodari L., Ballirano P., 2019. Chemical and structural characterization of UICC crocidolite fibres from Koegas Mine, Northern Cape (South Africa). Periodico di Mineralogia 88, 297-306.

Pascolo L., Borelli V., Canzonieri V., Gianoncelli A., Birarda G., Bedolla D.E., Salomé M., Vaccari L., Calligaro C., Cotte M., Hesse B., Luisi F., Zabucchi G., Melato M., Rizzardi C., 2015. Differential protein folding and chemical changes in lung tissues exposed to asbestos or particulates. Scientific reports 5, 12129.

Pascolo L., Gianoncelli A., Kaulich B., Rizzardi C., Schneider M., Bottin C., Polentarutti M., Kiskinova M., Longoni A., Melato M., 2011. Synchrotron soft X-ray imaging and fluorescence microscopy reveal novel features of asbestos body morphology and composition in human lung tissues. Particle and Fibre Toxicology 8, 7.

Pascolo L., Gianoncelli A., Rizzardi C., de Jonge M., Howard D., Paterson D., Cammisuli F., Salomé M., De Paoli P., Melato M., Canzonieri V., 2016a. Focused X-Ray Histological Analyses to Reveal Asbestos Fibers and Bodies in Lungs and Pleura of Asbestos-Exposed Subjects. Microscopy and Microanalysis 22, 1062-1071.

Pascolo L., Gianoncelli A., Schneider G., Salomé M., Schneider M., Calligaro C., Kiskinova M., Melato M., Rizzardi C., 2013. The interaction of asbestos and iron in lung tissue revealed by synchrotron-based scanning X-ray microscopy. Scientific Reports 3, 1123.

Pascolo L., Zabucchi G., Gianoncelli A., Kourousias G., Trevisan E., Pascotto E., Casarsa C., Ryan C., Lucattelli M., Lungarella G., Cavarra E., Bartalesi B., Zweyer M., Cammisuli F., Melato M., Borelli V., 2016b. Synchrotron X-ray microscopy reveals early calcium and iron interaction with crocidolite fibers in the lung of exposed mice. Toxicology Letters 241, 111-120.

Paunesku T., Wanzer M. B., Kirillova E. N., Muksinova K.N., Revina V.S., Lyubchansky E.R., Grosche B., Birschwilks M., Vogt S., Finney L., Woloschak G.E., 2012. X-ray fluorescence microscopy for investigation of archival tissues. Health Physics 103, 181-186.

Perrin L., Carmona A., Roudeau S., Ortega R., 2015. Evaluation of sample preparation methods for single cell quantitative elemental imaging using proton or synchrotron radiation focused beams. Journal of Analytical Atomic Spectrometry 30, 2525-2532.

Petriglieri J.R., Salvioli-Mariani E., Mantovani L., Tribaudino M., Lottici P.P., Laporte-Magoni C., Bersani D., 2015. Micro-Raman mapping of the polymorphs of serpentine. Journal of Raman Spectroscopy 46, 953-958.

Pollastri S., Gualtieri A.F., Vigliaturo R., Ignatyev K., Strafella E., Pugnaloni A., Croce A., 2016b. Stability of mineral fibres in contact with human cell cultures. An in situ μXANES, μXRD and XRF iron mapping study. Chemosphere 164, 547-557.

Pollastri S., Perchiazzi N., Lezzerini M., Plaisier J.R., Cavallo A., Dalconi M. C., Gandolfi N.B., Gualtieri A.F., 2016a. The crystal structure of mineral fibres: 1. Chrysotile. Periodico di Mineralogia 85, 249-259.

Porcaro F., Roudeau S., Carmona A., Ortega R., 2018. Advances in element speciation analysis of biomedical samples using synchrotron-based techniques. TrAC Trends in Analytical Chemistry 104, 22-41.

Punshon T., Chen S., Finney L., Howard L., Jackson B.P., Karagas M.R., Ornvold K., 2015. High-resolution elemental mapping of human placental chorionic villi using synchrotron X-ray fluorescence spectroscopy. Analytical and bioanalytical chemistry 407, 6839-6850.

Rinaudo C., Belluso E., Gastaldi D., 2004. Assessment of the use of Raman spectroscopy for the determination of amphibole asbestos. Mineralogical Magazine 68, 455-465.

Salomé M., Cotte M., Baker R.P., Barrett R., Benseny-Cases N., Berruyer G., Bugnazet D., Castillo-Michel H., Cornu C., Fayard B., Gagliardini E., Hino R., Morse J., Papillon E., Pouyet E., Rivard C., Solé V. A., Susini J., Veronesi G., 2013. The ID21 Scanning X-ray Microscope at ESRF. Journal of Physics: Conference Series 425, 182004.

Sarret G., Pilon Smits E., Castillo Michel H., Isaure M., Zhao F., Tappero R., 2013. Use of synchrotron-based techniques to elucidate metal uptake and metabolism in plants. Advances in Agronomy 119, 1-82.

Solé V.A., Papillon E., Cotte M., Walter, Ph., Susini J., 2007. A multiplatform code for the analysis of energy-dispersive X-ray fluorescence spectra. Spectrochimica Acta Part B Atomic Spectroscopy 62, 63-68.

Vogel-Mikuš K., Pongrac P., Pelicon P., Vavpetič P., Povh B., Bothe H., Regvar M., 2009. Micro-PIXE analysis for

localization and quantification of elements in roots of Mycorrhizal metal-tolerant plants. In: Varma, A., Kharkwal, A.C. (Eds.), Symbiotic Fungi: Principles and Practice. Springer Berlin Heidelberg, Berlin, Heidelberg, 227-242.

Zohdi V., Whelan D.R., Wood B.R., Pearson J.T., Bambery K.R., Black M.J., 2015. Importance of tissue preparation methods in FTIR micro-spectroscopical analysis of biological tissues: 'Traps for new users'. PLoS ONE 10(2), e0116491.